Neutrophil-driven CD206^{hi}MHCII^{lo} macrophages are critical for skin fibrosis during systemic sclerosis

Yufang shi (yfshi@suda.edu.cn)
Pixia Gong
Suzhou Medical College of Soochow University
Yayun Ding
Suzhou Medical College of Soochow University
Wen Li
Suzhou Medical College of Soochow University
Xiao Su
Suzhou Medical College of Soochow University
Ruifeng Tian
Suzhou Medical College of Soochow University
Yipeng Zhou
Suzhou Medical College of Soochow University
Tingting Wang
Soochow University
Junjie Jiang
Suzhou Medical College of Soochow University
Rui Liu
Soochow University
Jiankai Fang
Soochow University
Chao Feng
Suzhou Medical College of Soochow University
Changshun Shao
Soochow University https://orcid.org/0000-0003-2618-9342
Peishan Li
Suzhou Medical College of Soochow University

Article

Keywords: systemic sclerosis, neutrophils, CD206hiMHCIIlo macrophages, NETs, MerTK

Posted Date: July 11th, 2022

DOI: https://doi.org/10.21203/rs.3.rs-1819715/v1

Abstract

Systemic sclerosis (SSc) is a recalcitrant autoimmune disease characterized by progressive fibrosis in the skin and internal organs, such as the lungs. A key feature of this disease is the infiltration of innate immune cells, yet, how they contribute to the pathogenesis of SSc is largely unknown. Here, we demonstrated that the $CD206^{hi}MHCII^{lo}$ macrophages were the dominant immune cell population accumulated in the fibrotic skin of SSc mice, and these cells were found to be critical in mediating the profibrotic response by producing TGF-β1 in a MerTK signaling-dependent manner. Interestingly, the neutrophil infiltration was a prerequisite for the accumulation of $CD206^{hi}MHCII^{lo}$ macrophages and depletion of neutrophils or inhibition of CXCR1/2 could reduce $CD206^{hi}MHCII^{lo}$ macrophages and alleviate SSc progression. Detailed investigations revealed that in the fibrotic skin, neutrophils released neutrophil extracellular traps (NETs) ensnared macrophages and were responsible for the differentiation of $CD206^{hi}MHCII^{lo}$ macrophages. Our findings uncovered a key role of the neutrophil-macrophage-fibrosis axis in the pathogenesis of SSc and provide critical information for the development of novel therapeutic strategies.

Introduction

Systemic sclerosis (SSc), also known as scleroderma, is a complex autoimmune disease characterized by vascular injury, dysregulation of immune response, and ultimately severe fibrosis in the skin and internal organs [1]. Fibrosis is believed to be a result of uncontrolled tissue repair responses. Unlike the normal wound healing process, the SSc associated fibrosis is related to deregulated cellular responses and the sustained release of various cellular components and factors [2]. However, the dynamics and activities of the participating immune cells and their manners in mediating the skin fibrosis process during SSc are still largely unexplored.

It has been indicated that the infiltration of innate immune cells is associated with the pathogenesis of skin fibrosis during SSc [3]. Macrophages, in particular, have been recognized as key contributors to various fibrotic diseases [2], although their roles in SSc have not been defined. Macrophages are a heterogeneous cell population with different phenotypes and functions. Recent molecular and metabolic studies have revealed as many as six populations of tissue macrophages [4]. From the immunological point of view, macrophages can be divided into pro-inflammatory (M1) and anti-inflammatory (M2) populations [5]. In the presence of LPS and/or IFN-γ, monocytes can become pro-inflammatory macrophages, which are responsible for the inflammatory response during the initial phase of tissue damage [6]. On the other hand, in the presence of IL-4 and/or IL-13, monocytes are alternatively activated to become anti-inflammatory macrophages, which are believed to resolve inflammation and to carry out tissue reparative functions [6]. Failure in timely converting the pro-inflammatory responses to reparative responses is believed to be a major cause of impaired tissue repair and subsequently fibrosis [5]. Notably, although the anti-inflammatory macrophages are necessary for initiating the tissue repair program, persistent activation or sustained recruitment of these macrophages could also contribute to the initiation

and progression of fibrosis through aberrant secretion of various growth factors, such as transforming growth factor β (TGF-β) [7], vascular endothelial growth factor (VEGF) [8], and platelet-derived growth factor (PDGF) [9]. Thus, the responses mediated by distinct macrophage phenotypes need to be precisely regulated to permit normal tissue repair and to prevent fibrosis.

The definition of functional phenotypes of macrophages during the pathogenesis of SSc remains controversial. There are reports that “M2” macrophages positive for CD206, CD163, and CD204 are activated and functionally profibrotic in SSc patients [10-13]. Upregulated IL-4 and IL-13 levels in serum were also demonstrated [14]. However, there are studies indicating that “M1” macrophages positive for CD80, CD86, and TLR4 were also increased in peripheral blood of SSc patients [15-17]. These findings strongly suggest the dynamics of macrophage subset involvement during the SSc progression is complex. Detailed investigations may provide critical information for the understanding of the pathogenesis of SSc.

To elucidate the functions of various immune cell populations, we established the bleomycin-induced mouse model of SSc, which has been widely used to investigate the pathogenesis and therapies of SSc [18]. We demonstrated that $CD206^{hi}MHCII^{lo}$ macrophages were key contributors to skin fibrosis during SSc. These macrophages promoted skin fibrosis through expressing MerTK, which was required for TGF-β1 production. Additionally, neutrophil released NETs were responsible for the emergence of $CD206^{hi}MHCII^{lo}$ macrophages and their enhanced MerTK expression. Our results, therefore, revealed a novel role of the neutrophil-macrophage-fibrosis axis in the development of SSc.

Materials And Methods

Animals

BALB/c female mice (6-8 weeks) were purchased from Shanghai SLAC Laboratory Animal Co. Ltd. (Shanghai, China). Mice were housed in cages with a constant-flow air exchange to support the specific pathogen-free condition, with sterile water and irradiated food from Pu Lu Teng Biotechnology Co. Ltd. (Shanghai, China) provided ad libitum. Animal care was in full compliance with the Guide for the Care and Use of Laboratory Animals and the experimental protocols were approved by the Institutional Animal Care and Use Committee of Soochow University.

Animal experiments

Bleomycin sulfate (BLM) (Abmole, M2100) was dissolved in sterile phosphate-buffered saline (PBS) at a concentration of 1 mg/mL. Mice received daily intracutaneous injections (i.c.) of 100 μL bleomycin into their shaved backs (the para-midline, lower back region) for 4 weeks, and mice injected with 100 μL PBS were used as a control group.

In the macrophage ablation experiment, mice were i.p. injected with 100 μL clodronate liposome (5 mg/mL, Yeasen) or 100 μL control liposome 3 days before the first bleomycin challenge and then

administered every 4 days for 4 weeks. In the separate MerTK inhibition study, mice were daily i.p. injected with UNC2250 (5 mg/kg in 2% DMSO/30% PEG300/68% ddH_2O, 1493694-70-4, Selleck) or vehicle control (2% DMSO/30% PEG300/68% ddH_2O) from day 0 for 4 weeks.

In the neutrophil depletion experiment, mice were intraperitoneally injected (i.p.) with anti-Ly6G antibody (0.5 mg/kg in 200 μL PBS, BioLegend) or IgG2b isotype (0.5 mg/kg in 200 μL PBS, BioLegend) from day 3 after the first bleomycin challenge and injected every 4 days for 4 weeks. In a separate CXCR1/2 inhibition study, mice were i.p. injected with Reparixin (5 mg/kg in 2% DMSO/98% PBS, 266359-83-5, Selleck) or vehicle control (2% DMSO/98% PBS) from day 0 (the day of the first bleomycin challenge) for 4 weeks. In the experiment of NETs degradation by DNase I, mice were i.p. injected with 450 U DNase I in 200 μL PBS (D8071, Solarbio) or PBS from day 0, and injected every 2 days for 4 weeks.

Skin single cell acquisition

Mice were euthanized on day 30, the shaved back skin was removed and kept in PBS with 1% fetal bovine serum (FBS, Gibco) on ice. After scraping subcutaneous fat with forceps, the remaining skin was cut into pieces by surgical scissors as small as possible. Then the skin pieces were resuspended in Dulbecco's Modified Eagle Medium (DMEM, SH30021.01, HyClone) containing 10% FBS, 1% penicillin and streptomycin (PS, 15140163, Thermo Fisher Scientific), 0.25% type I collagenase (17100017, Gibco) and 0.01% DNase I (D8071, Solarbio) and digested for 2 h at 37°C. Next, the single cells from the digested skin tissues were filtered through a 70 μm strainer, and centrifuged at 300×g for 5 min. The precipitate was washed 1 or 2 times with 10 mL PBS. Finally, skin cells were resuspended in 1 mL PBS containing 1% FBS for subsequent experiments.

Flow cytometry

Single mouse skin cells as prepared above were first stained with Fixable Viability Stain 700 (564997, BD Pharmingen) to exclude dead cells. For cell-surface protein staining, cells were blocked with anti-mouse CD16/CD32 antibody (553141, BD Pharmingen) and then stained with the indicated antibodies for 30 min at 4°C in FACS buffer (PBS containing 1% FBS). For staining of intracellular proteins, cells were fixed and permeabilized with a Foxp3/Transcription Factor Staining Buffer Set Kit (00-5523-00, eBioscience) for 30 min at 4°C, followed by incubation with the indicated antibodies for 30 min at 4°C in Permeabilization buffer (00-5523-00, eBioscience). Cell phenotyping was performed on the Cytoflex Flow Cytometer (Beckman Coulter, U.S.A.). Cell sorting was performed on a MoFlo AstriosEQ (Beckman Coulter, U.S.A.), the purity of sorted cells was consistently above 95% for each sample. Data were analyzed using Flow Jo software (Version 10.0.7, Tree Star Inc.). Cell-surface antibodies used were as follows: PE/Cyanine7 anti-mouse CD45 (103114, BioLegend), Brilliant Violet 510 anti-mouse CD45 (563891, BD Pharmingen), PerCP/Cyanine5.5 anti-mouse CD45 (103132, BioLegend), APC/Cyanine7 rat anti-CD11b (557657, BD Pharmingen), PE/Cyanine7 anti-mouse CD24 (101822, BioLegend), PerCP/Cyanine5.5 anti-mouse CD24 (101824, BioLegend), Brilliant Violet 605 anti-mouse Ly-6G (127639, BioLegend), Brilliant Violet 510 anti-mouse Ly-6G (127633, BioLegend), FITC anti-mouse Ly-6G (127606, BioLegend), Brilliant

Violet 421 anti-mouse Ly-6C(128031, BioLegend), PE anti-mouse Ly-6C(128007, BioLegend), FITC anti-mouse CD64 (139316, BioLegend), APC anti-mouse CD64 (139306, BioLegend), Brilliant Violet 605 anti-mouse I-A/I-E (107639, BioLegend), PE-Cyanine7 anti MerTK (25575182, eBioscience), Brilliant Violet 510 anti-mouse F4/80 (123135, BioLegend). Intracellular antibodies were as follows: Brilliant Violet 421 anti-mouse CD206 (MMR) (141717, BioLegend), APC anti-mouse CD206 (MMR) (141708, BioLegend), PE anti-mouse Arg-1 (12-3697-82, eBioscience), APC anti-mouse Arg-1 (17-3697-82, eBioscience) and PE anti-mouse NOS2 (12-5920-82, eBioscience).

RNA Sequencing

To obtain highly purified $CD206^{hi}MHCII^{lo}$ and $CD206^{lo}MHCII^{hi}$ macrophages to perform RNA sequencing, skin single cells were first subjected to $CD45^{+}$ total immune cell isolation by CD45 MicroBeads (130-052-301, Miltenyi Biotec) according to the manufacturer's specifications. Then the isolated $CD45^{+}$ cells were used for fluorescence-activated cell sorting to further isolate the macrophage subsets of $CD206^{hi}MHCII^{lo}$ and $CD206^{lo}MHCII^{hi}$. The 2 purified macrophage subsets (10,000-20,000 cells per sample) were lysed in TRIzol Reagent (15596-08, Life Technologies) and sent to LC Sciences (China) for RNA sequencing.

Hematoxylin-eosin and Sirius red staining

Skin samples from the mouse lower back were excised and fixed with 4% paraformaldehyde for 24 h, dehydrated with 70%, 75%, 85%, 95%, 100% ethyl alcohol, and then embedded into paraffin. 5 μm thick sections were stained with hematoxylin and eosin. Skin thickness was defined as the length from the top of the granular layer to the junction between the dermis and subcutaneous fat. A picrosirius red staining kit (PSR-1, ScyTek) was used to visualize dermal collagen according to the manufacturer's instructions. Collagen content was defined as the distance from the top of the dermal layer to the junction between the dermis and subcutaneous fat.

Immunofluorescence staining

For immunofluorescence staining, slides were subjected to antigen retrieval in Tris-EDTA, pH 9.0 (R20904, Yuanye Bio-Technology), at 96°C for 30 min. Then slides were treated with 3% bovine serum albumin (BSA, CCS30014.02, MRC) for 1 h before incubation with primary antibodies overnight at 4°C. On the next day, sections were washed with PBS 3 times and incubated with the secondary antibodies for 1 h at room temperature. The nuclei were stained with Hoechst 33324 (H3570, Thermo Fisher Scientific). The primary antibodies used were as follows: anti-α-smooth muscle actin (α-SMA) (ab124964, Abcam), anti-CD64 (MA529704, Invitrogen), anti-CD64 (139302, BioLegend), anti-Ly6G (ab25377, Abcam), anti-Histone H3 (citrulline R2 + R8 + R17) (cit-H3) (ab5103, Abcam), anti-Mer (AF591, R&D) and anti-TGF-β1 (ab215715, Abcam). The secondary antibodies were Alexa Fluor 488-conjugated-goat anti-rabbit IgG (ab150077, Abcam), Alexa Fluor 594-conjugated-goat anti-rat IgG (ab150160, Abcam), Alexa Fluor 555-conjugated-donkey anti-goat IgG (A-21432, Thermo Fisher Scientific), and Alexa Fluor 647-conjugated-goat anti-rabbit

IgG (ab150083, Abcam). Images were captured under a laser-scanning confocal microscope (Leica TCS SP8, Leica, Germany).

Western blotting

Skin tissues were lysed in RIPA buffer (P0013B, Beyotime) in the presence of protease inhibitors. Equal amounts of protein lysate samples were resolved by sodium dodecyl sulfate polyacrylamide gel electrophoresis and then transferred onto polyvinylidene fluoride membranes. After blocking with 5% BSA in Tris-buffered saline containing 0.1% Tween 20 for 1 h, the membranes were incubated at 4°C overnight with respective primary antibodies. Membranes were washed 3 times followed by incubation with horseradish peroxidase-conjugated secondary antibody for 1 h at room temperature. Signals were visualized by an NcmECL Ultra kit (P10300, NCM Biotech) with a FluorChem E system (Protein Simple, U.S.A.). The primary antibodies used were as follows: anti-Histone H3 (citrulline R2 + R8 + R17) (cit-H3) (ab5103, Abcam), and anti-Gas6 (67202S, CST).

Induction of NETs

Total neutrophils from mouse bone marrow were obtained by negative selection using the Mouse Neutrophil Isolation Kit (130-097-658, Miltenyi Biotec) according to the manufacturer's specifications. NETs were induced by overnight stimulation of neutrophils with 20 μmol/mL phorbol 12-myristate 13-acetate (PMA) (P1585, Sigma Aldrich) and 100 ng/mL LPS (L2630, Sigma Aldrich). Sytox Green dead cell stain (R37109, Thermo Fisher) was added to label the induced NETs 20 min before collection. Then the deposited NETs layer at the bottom of the culture dish was washed 4 times in PBS and collected by vigorous pipetting with 1640 medium. Cell debris was removed by centrifugation at 300g for 10 min and the supernatant containing NETs was stored at -80°C for further use.

Co-culture of macrophages and NETs

Bone marrow-derived monocytes (BMDMs) were acquired as previously described [19]. Briefly, bone marrow cells were flushed from the femurs and tibia of BALB/c mice and subjected to red blood cell lysis. Cells were passed through a 40 μm strainer and cultured in DMEM/F12 (03.2001C, EallBio) medium with 10% FBS, 1% PS and 10 ng/mL recombinant murine M-CSF (315-02, PeproTech) for 7 days. Then matured macrophages were co-cultured with or without NETs for 24 h, in the presence or absence of M1 stimuli: 100 ng/mL LPS (L2630, Sigma Aldrich) and 10 ng/mL IFN-γ (NBP2-35071, NOVUS); or M2 stimuli: 20 ng/mL IL-4 (214-14-20, PeproTech) and 20 ng/mL IL-13 (NBP2-35103, NOVUS). In the NETs degradation experiment, NETs were pre-treated with 20 U/mL DNase I for 2 h at 37°C.

Skin single-cell suspensions were obtained as described above. Then, skin cells were co-cultured with or without NETs or DNase I-treated NETs for 24 h in the presence of M2 stimuli: 20 ng/mL IL-4 (214-14-20, PeproTech) and 20 ng/mL IL-13 (NBP2-35103, NOVUS).

Detection of cytokines

The levels of IL-4 and IL-13 in skin homogenate were assayed by ELISA kits: mouse anti-IL-4 ELISA kit (abs520003, Absin) and mouse anti-IL-13 ELISA kit (abs520012, Absin). 10 mg skin tissue from the backs of the mice was removed and weighed. Then skin tissues were homogenized in 200 μL PBS with protease inhibitors. The supernatant was obtained and tested according to the manufacturer's instructions.

Statistical analysis

Statistical analyses were performed by Prism 9 (GraphPad Software). Data are presented as the mean ± SEM in the animal experiments or the mean ± SD in the cell experiments. For comparisons between the two groups, P-values by unpaired Student's t test were reported if normality of the data could be confirmed by Shapiro-Wilk tests; otherwise, the Mann-Whitney U test was used. For comparisons among multiple groups, one-way ANOVA followed by Tukey's multiple comparison test was used. A P-value lower than 0.05 is considered significant. *$P < 0.05$; **$P < 0.01$, ***$P < 0.001$; ns, not significant.

Results

Macrophages are key contributors to skin fibrosis during SSc

An animal model of SSc was induced in BALB/c mice by daily bleomycin (BLM) injection for 4 weeks. The skin was first examined histologically, and typical disease processes starting with inflammation at even 2 hours and progression to fibrosis after 2 weeks were observed (data not shown). To determine the changes in immune cell populations, we analyzed skin resident immune cells by flow cytometry on day 30 after SSc fully developed. Skin tissue was digested, and the mixed cell population was subjected to flow cytometry using the gating strategy outlined in Fig S1 [20, 21]. Among various populations of immune cells identified, macrophages and neutrophils were most significantly increased (Fig S1). Macrophages ($CD11b^+CD64^+$) accounted for approximately 30% of the total $CD45^+$ immune cells in the skin of control mice, while macrophages reached approximately 50% in BLM-treated mice (Fig S2A). On the other hand, neutrophils ($CD11b^+Ly6G^+$), which are relatively rare in control mice (approximately 1%), increased approximately 5-fold in bleomycin treated mice (Fig S2B). It is important to point out that Langerhans cells ($CD11b^+CD24^+$) and B cells ($CD19^+$) were hardly altered after BLM challenge (Fig S2C and S2D, right). In addition, the percentages of dendritic cells ($CD11b^+Ly6G^-CD24^-CD64^-Ly6C^-$) and T cells ($CD3^+$) were significantly decreased in total immune cells, due to the substantial increase in macrophages and neutrophils (Fig S2E and S2D, left).

We further examined the distribution of macrophages in the skin lesions by immunofluorescence staining of CD64 and found that the infiltrated $CD64^+$ cells mostly accumulated in the dermis of BLM-treated mice (Fig 1A). To determine the profibrotic role of macrophages, we depleted them with clodronate liposomes (Clo). Clo or control liposomes (Ctrl) were administered intraperitoneally starting on day 3 prior to BLM treatment and repeated every 4 days throughout the whole course of SSc induction (Fig 1B). Clo effectively ablated skin macrophages in BLM-treated mice (Fig 1C) and attenuated the increase in skin thickness and collagen deposition, as shown by H&E staining (Fig 1D) and Sirius red staining (Fig 1E). α-

SMA staining, a hallmark of fibrosis, also revealed the impediment of skin fibrosis after Clo treatment (Fig 1F). These results clearly demonstrated that macrophages are a key contributor to the development of skin fibrosis during SSc.

$CD206^{hi}MHCII^{lo}$ macrophages promote SSc skin fibrosis via MerTK signaling

Macrophages can differentiate toward certain functional phenotypes according to environmental cues. The role of pro-inflammatory and anti-inflammatory macrophages in the development of fibrosis is controversial [6]. To determine the phenotype related function of macrophages in skin fibrosis of BLM-induced SSc, we analyzed the markers of skin macrophages by flow cytometry to determine the responsible subset. Skin macrophages ($CD11b^{+}CD64^{+}$) were divided into two populations based on the expression of CD64 and Ly6C (Fig 2A, left). The $CD64^{+}Ly6C^{+}$ population possessed mixed markers of macrophages ($CD64^{+}$) and monocytes ($Ly6C^{+}$), which could be regarded as maturing macrophages representing a transition state from monocytes to macrophages, while the $CD64^{+}Ly6C^{-}$ population was regarded as matured macrophages. These 2 macrophage populations could be further classified into distinct subsets according to the expression of CD206 (expressed mainly on anti-inflammatory macrophages) and MHCII (expressed mainly on pro-inflammatory macrophages). As such, 2 subsets of $CD64^{+}Ly6C^{+}$ maturing macrophages, $CD206^{-}MHCII^{-}$ and $CD206^{lo}MHCII^{hi}$ (Fig 2A), and 4 subsets of $CD64^{+}Ly6C^{-}$ matured macrophages, $CD206^{-}MHCII^{-}$, $CD206^{lo}MHCII^{hi}$, $CD206^{hi}MHCII^{hi}$ and $CD206^{hi}MHCII^{lo}$ (Fig 2B), were observed in control mice. The subsets of $CD64^{+}Ly6C^{+}$ maturing macrophages exhibited no significant change after BLM challenge (Fig 2A). In contrast, the subsets of $CD64^{+}Ly6C^{-}$ matured macrophages were remarkably altered. On the one hand, the $CD206^{hi}MHCII^{hi}$ subset almost disappeared. On the other hand, the $CD206^{hi}MHCII^{lo}$ subset was significantly increased (Fig 2B). It is necessary to emphasize that the $CD206^{hi}MHCII^{lo}$ macrophages were analogous to the so called M2 macrophages according to the high expression of CD206 and low MHCII expression. We therefore examined the expression of Arg-1, a marker of M2 macrophages, in the 4 subsets of $CD64^{+}Ly6C^{-}$ matured macrophages. Arg-1 positive cells increased significantly after BLM treatment in all 4 subsets, but the most pronounced increase was seen in the $CD206^{hi}MHCII^{lo}$ subset (Fig 2C), shich was the main $Arg\text{-}1^{+}$ cells among $CD64^{+}Ly6C^{-}$ matured macrophages (Fig 2D).

Anti-inflammatory M2-like macrophages have potent phagocytic capability to clean up dead cells and debris through TAM receptors (Tyro3, Axl, and MerTK) during tissue homeostasis maintenance. However, hyper-activation of the TAM receptors has also been linked to tissue fibrosis [22]. MerTK activation has been shown to promote the production of TGF-β1 [23]. Therefore, we speculated that $CD206^{hi}MHCII^{lo}$ macrophages might contribute to skin fibrosis by continuously engaging in phagocytosis. As expected, the key phagocytic receptor MerTK was upregulated significantly in all 4 subsets of $CD64^{+}Ly6C^{-}$ matured macrophages in BLM treated mice (Fig 2E). On the other hand, $CD64^{+}Ly6C^{+}$ maturing macrophages expressed less MerTK (Fig S3A). Among the $CD64^{+}Ly6C^{-}$ cells, $CD206^{hi}MHCII^{lo}$ macrophages showed highest expression of MerTK (Fig 2F). Interestingly, Gas6, a ligand of MerTK, was found to be

significantly increased in the skin lysates of BLM-treated mice (Fig 2G), further indicating the role of MerTK in SSc skin fibrosis.

Animals have evolved highly efficient mechanisms to clean-up dead cells and at a given time, most experimental protocols can only capture a snapshot of the removing process. To investigate whether $CD206^{hi}MHCII^{lo}$ macrophages are indeed involved in phagocytosis during the pathogenesis of skin fibrosis, we isolated the 2 major macrophage subsets in the fibrotic skin, $CD206^{hi}MHCII^{lo}$ and $CD206^{lo}MHCII^{hi}$, from BLM treated mice and performed RNA sequencing to interrogate the activation of the phagocytic pathways. KEGG and GO analyses showed substantial differences between the 2 subsets. The pathways related to phagosomes in the KEGG analysis and the “phagocytic vesicle membrane” pathways in the GO analysis were among the upregulated biological pathways in the $CD206^{hi}MHCII^{lo}$ subset compared with the $CD206^{lo}MHCII^{hi}$ subset (Fig S3B), suggesting the higher phagocytic ability of $CD206^{hi}MHCII^{lo}$ macrophages.

To determine whether the upregulated MerTK signaling in $CD206^{hi}MHCII^{lo}$ macrophages contributes to their profibrotic capability, we subjected BLM challenged mice with MerTK inhibitor UNC2250 intraperitoneally. The treatment was performed daily starting on day 0 for the entire course of SSc induction (Fig 2H). Skin thickness and collagen content were significantly reduced in the UNC2250-treated group compared to the DMSO- treated group, as shown by H&E staining (Fig 2I) and Sirius red staining (Fig 2J). α-SMA staining also verified the attenuation of fibrosis in the UNC2250 treated group (Fig 2K). It has been reported that MerTK activation could lead macrophages to exhibit an anti-inflammatory M2-like phenotype [24]. We therefore determined whether MerTK mediates the polarization of $CD206^{hi}MHCII^{lo}$ macrophages. UNC2250 treatment did not affect the abundance of $CD206^{hi}MHCII^{lo}$ macrophages (Fig 2L). However, MerTK was found to be highly colocalized with TGF-β1 (Fig 2M) and UNC2250 treatment significantly reduced the expression of TGF-β1 in $CD206^{hi}MHCII^{lo}$ macrophages (Fig 2N). Based on these results, we concluded that upregulation of MerTK signaling is associated with the induction of TGF-β1 expression in $CD206^{hi}MHCII^{lo}$ macrophages that play a key role in skin fibrosis during SSc.

Neutrophil depletion inhibits the differentiation of $CD206^{hi}MHCII^{lo}$ macrophages

Neutrophils first accumulated in skin lesions as early as 2 h after BLM treatment, which were immediately followed by macrophages (Fig 3A). Both neutrophils and macrophages infiltrated at high rates during the first 3 days of SSc induction, representing the early inflammatory phase. Fibrosis started from the second to fourth weeks, during which neutrophils persisted, albeit at a relatively lower frequency. On the other hand, the macrophage density remained high. This kinetics suggested that neutrophils may act in concert with macrophages during SSc progression. Indeed, it has been shown that during lung and heart tissue injury, neutrophils reprogram macrophages toward an M2-like phenotype by secreting factors or through the “efferocytosis” process [25]. Thus, we investigated the effects of neutrophils on the differentiation or recruitment of macrophages during SSc. We depleted neutrophils with an anti-Ly6G antibody (Fig 3B). To

examine the role of neutrophils on macrophages during the inflammatory phase and the fibrogenic phase, anti-Ly6G was administered intraperitoneally on 2 schedules: one started on day 3 followed by every 4 days, and another started on day 10 followed by every 4 days (Fig 3C). Neutrophil depletion caused a significant decrease in $CD206^{hi}MHCII^{lo}$ macrophages in both experimental schemes, indicating that neutrophils were essential for the differentiation of $CD206^{hi}MHCII^{lo}$ macrophages (Fig 3D). However, neutrophil depletion had no effect on the percentage of total macrophages (Fig 3E, left). Further analysis showed that neither $CD64^{+}Ly6C^{+}$ maturing macrophages nor $CD64^{+}Ly6C^{-}$ matured macrophages were affected by neutrophil depletion (Fig 3E, middle and right). Importantly, neutrophil depletion attenuated skin fibrosis, as shown by significantly decreased skin thickness (Fig 3F) and collagen deposition (Fig 3G). The expression of α-SMA also significantly decreased in neutrophil depletion (Fig 3H). These results indicate that neutrophil depletion inhibits the differentiation of fibrosis-promoting $CD206^{hi}MHCII^{lo}$ macrophages.

Inhibition of CXCR1/2 reduced $CD206^{hi}MHCII^{lo}$ macrophages

The chemoattractant-chemokine receptor axis is responsible for the recruitment of neutrophils. CXCR1 and CXCR2 are major chemokine receptors expressed on neutrophils and these receptors can be activated by ELR-positive CXC chemokines, including CXCL1, 2, and 3 and CXCL5, 6, 7, and 8 [26]. These chemokines not only mediate the migration of neutrophils into the inflamed site, but also promote the release of neutrophils from bone marrow [27]. To further clarify the role of recruited neutrophils in promoting the polarization of $CD206^{hi}MHCII^{lo}$ macrophages, we also tested the effect of the CXCR1/2 inhibitor Reparixin. Reparixin or DMSO was administered intraperitoneally daily to BLM treated or untreated mice starting from day 0 for the entire course of SSc induction (Fig 4A). Reparixin not only strongly inhibited the infiltration of neutrophils into the skin (Fig 4B), but also reduced neutrophils in the spleen (Fig 4C). CXCR1/2 inhibition by Reparixin could also significantly reduce the percentage of $CD206^{hi}MHCII^{lo}$ macrophages (Fig 4D). The neutrophil reduction induced by Reparixin treatment did not affect the percentage of total macrophages (Fig 4E, left). Additionally, the percentage of neither $CD64^{+}Ly6C^{+}$ maturing macrophages nor $CD64^{+}Ly6C^{-}$ matured macrophages was influenced by Reparixin treatment (Fig 4E, middle and right). Skin thickness, collagen content, and α-SMA expression were all significantly decreased in the reparixin-treated group, as shown by H&E staining (Fig 4F), Sirius red staining (Fig 4G), and α-SMA immunofluorescence staining (Fig 4H). These results clearly demonstrate that CXCR1/2-mediated neutrophil recruitment is critical for $CD206^{hi}MHCII^{lo}$ macrophage-mediated skin fibrosis.

Neutrophil-released NETs promote the differentiation of $CD206^{hi}MHCII^{lo}$ macrophages

We then explored the mechanism through which neutrophils confer profibrotic properties to macrophages. Neutrophils are short lived, and one way they die is through NETosis, during which NETs are released. We therefore examined the existence of NETs in fibrotic skin. We found that the marker for NETs, citrullinated histone 3 (cit-H3), was significantly increased in the skin of BLM treated mice, as

shown by immunofluorescence staining analysis (Fig 5A) and western blotting analysis (Fig 5B). To directly test the role of NETs, we induced NETs in bone marrow derived neutrophils by PMA and LPS treatment in vitro and co-cultured them with bone marrow-derived macrophages (BMDMs) for 24 h (Fig 5C). The expression levels of MerTK, Arg-1, and CD206, which were found to be highly expressed on $CD206^{hi}MHCII^{lo}$ macrophages in the in vivo experiments, were specifically examined. Interestingly, NETs alone increased the expression of MerTK (Fig 5D), but did not change the expression of Arg-1 on macrophages (Fig 5E). However, in the presence of IL-4 and IL-13, NETs further increased MerTK (Fig 5F), and also significantly enhanced the expression of Arg-1 (Fig 5G). The effects of NETs on MerTK and Arg-1 expression were abolished by DNase I treatment (Fig 5H and 5I). However, NETs did not alter the expression of CD206 either alone (Fig S4A) or in combination with IL-4 and IL-13 (Fig S4B).

To further verify the effect of NETs on skin $CD206^{hi}MHCII^{lo}$ macrophages, we made a single-cell suspension from dorsal skin of healthy mice with NETotic neutrophils in the presence of IL-4 and IL-13 (Fig 5J) and found that NETs in combination with IL-4 and IL-13 significantly augmented the polarization of $CD206^{hi}MHCII^{lo}$ macrophages in the cell suspension (Fig 5K). This induction of $CD206^{hi}MHCII^{lo}$ macrophages was abolished by DNase I treatment (Fig 5K). Similarly, this combination also significantly increased the expression of MerTK and Arg-1, which were also abolished by DNase I treatment (Fig 5L and 5M). To determine the immune milieu in the fibrotic skin, we performed ELISA and observed that IL-4 and IL-13 in fibrotic skin were significantly increased (Fig 5N and 5O), suggesting that fibrotic skin can indeed predispose macrophages towards a $CD206^{hi}MHCII^{lo}$ population.

NETs play a critical role in skin fibrosis during SSc

To further verify the role of NETs in regulating $CD206^{hi}MHCII^{lo}$ macrophage driven skin fibrosis, we employed DNase I to degrade NETs in vivo. DNase I or PBS were administered intraperitoneally every other day starting on day 0 after SSc induction (Fig 6A). DNase I was effective in degrading NETs in vivo, as indicated by western blotting analysis (Fig 6B). Flow cytometry analysis showed that NETs degradation significantly reduced $CD206^{hi}MHCII^{lo}$ macrophages in the fibrotic skin (Fig 6C), but did not change total macrophages (Fig 6D, left). The percentage of neither $CD64^{+}Ly6C^{+}$ maturing macrophages nor $CD64^{+}Ly6C^{-}$ matured macrophages was affected by NETs degradation (Fig 6D, middle and right). Immunofluorescence staining of MerTK and TGF-β1 also showed their decrease upon DNase I treatment in SSc mice (Fig 6E). Importantly, DNase I treatment also significantly alleviated skin fibrosis as indicated by the reduced skin thickness (Fig 6F), collagen content (Fig 6G) and α-SMA expression (Fig 6H). These results further demonstrate that NETs generated by neutrophils play an important role in promoting SSc skin fibrosis by augmenting the polarization of $CD206^{hi}MHCII^{lo}$ macrophages.

Discussion

Various innate immune cell populations contribute to profibrotic responses in SSc, but the crosstalk among them is largely unknown [28]. In this study, we demonstrate that the $CD206^{hi}MHCII^{lo}$

macrophages are dominant immune cell population contributing to skin fibrosis by producing TGF-β1 in a MerTK signaling-dependent manner. Importantly, we find that neutrophil infiltration is a prerequisite for the accumulation of these CD206^{hi}MHCII^{lo} macrophages. Additionally, neutrophils promote the differentiation of CD206^{hi}MHCII^{lo} macrophages through NETosis. Depletion of neutrophils or degradation of NETs can reduce the population of CD206^{hi}MHCII^{lo} macrophages and subsequently alleviate SSc progression. Therefore, the crosstalk between neutrophils and macrophages is critical in the pathogenesis of SSc.

Macrophages have been reported to orchestrate tissue repair and to promote fibrosis under specific conditions. Macrophage-mediated profibrotic responses have been documented in various types of organs, including the liver, kidney, heart and lungs during infections or particular disease processes [5, 29]. However, there is a lack of consensus regarding the particular subtype or polarization status of macrophages that mediate the profibrotic responses. Some studies have shown that the hyperactivation of pro-inflammatory M1 macrophages leads to the development of pulmonary fibrosis [30], cardiac fibrosis [31] and liver fibrosis [32], while others have indicated that the hyper-activation of anti-inflammatory M2 macrophages is responsible for causing renal and skin fibrosis [33, 34]. This discrepancy may result from special tissue microenvironments, the causes and types of the inflammatory response as well as the pathogenesis episodes during which macrophages are examined. In our experimental setting, we observed that the CD206^{hi}MHCII^{lo} M2-like macrophages were the key profibrotic cell type during the development of BLM-induced skin fibrosis. A profibrotic function of M2 macrophages was also reported in a lung fibrosis model [35]. It seems that the phenotypes of macrophages can be converted between pro-inflammatory and anti-inflammatory during some abnormal tissue repair processes, rather than remaining unchanged throughout an entire repair process. It has been reported that blockade of the recruitment of pro-inflammatory monocytes using a CCR2 inhibitor could significantly alleviate BLM-induced skin fibrosis [36]. We speculate that during the early stage of SSc, the pro-inflammatory monocytes/macrophages may initiate the fibrotic response and this initial fibrotic response is followed by the accumulation of CD206^{hi}MHCII^{lo} macrophages that intensify this profibrotic process in the later stage. Further characterization of the drivers for the dynamic of pro-inflammatory macrophages and anti-inflammatory macrophages in mediating fibrosis will allow a better understanding of the roles of different macrophage populations in fibrosis development.

Macrophages are the main phagocytic cells. The activation of the phagocytic receptor MerTK has been shown to prevent the polarization of pro-inflammatory macrophages by attenuating inflammatory pathways [37-39] and thus confer macrophages the anti-inflammatory phenotype [24]. Excessive MerTK expression in macrophages has been determined to be a risk factor in several fibrotic disease systems. In idiopathic pulmonary fibrosis, SPP1^{hi}MerTK^{hi} macrophages are highly proliferative and profibrotic [40]. In IgG4-related disease, MerTK is highly expressed in infiltrated macrophages, and MerTK^{+} macrophages express high levels of the profibrotic factor TGF-β [41]. In nonalcoholic steatohepatitis- induced liver fibrosis, MerTK signaling in macrophages drives the expression of TGF-β1 to activate hepatic stellate cells to synthesize collagen [42]. In the present study, we demonstrated that MerTK was mainly expressed

in CD206^{hi}MHCII^{lo} macrophages and that MerTK-mediated phagocytic signaling drove the profibrotic response. We also found that MerTK signaling in CD206^{hi}MHCII^{lo} macrophages upregulated TGF-β1, thus promoting BLM-induced skin fibrosis. Further experiments using mice with MerTK-knockout specific in CD206^{hi}MHCII^{lo} macrophages would validate the exact role of MerTK in CD206^{hi}MHCII^{lo} macrophages during skin fibrosis. Notably, due to the anti-inflammatory property of the apoptotic cell phagocytosis pathway, impairment of such apoptotic cell removal process has been linked to the development of some autoimmune diseases, such as systemic lupus erythematosus, rheumatoid arthritis, and multiple sclerosis [43]. Consequently, the phagocytic signals are likely to be critical in regulating the interplay between inflammation and fibrosis [22]. Impairment in phagocytosis could lead to chronic inflammation, while excessive phagocytosis signals may cause fibrosis.

Type II T cell cytokines and phagocytosis have been reported to be responsible for the polarization and proliferation of M2-like macrophages [44]. However, we demonstrated that MerTK inhibition did not influence the polarization of CD206^{lo}MHCII^{hi} macrophages per se but rather specifically affected TGF-β1 production. The lack of an effect of the MerTK inhibitor on the polarization of CD206^{lo}MHCII^{hi} macrophages could be due to the presence of NETs and the lack of sufficient contacts of apoptotic cells in fibrotic skin. It is also possible that the effect of NETs overrides the effect of apoptotic cells on the polarization of CD206^{lo}MHCII^{hi} macrophages. Inflammatory stimulators, such as microbes, lipopolysaccharide, IL-8, and TNF-α, can serve as inducers of NETosis [45]. Presumably, during IL-4 and IL-13-mediated fibrosis, NETosis could be induced by molecules of damage-associated molecular patterns, such as released mtDNA through the STING and TLR9 pathways [46]. Type I interferons, which are highly upregulated in SSc patients, are also likely to induce NETosis [47]. During inflammatory diseases, NETs have been shown to promote the polarization of pro-inflammatory macrophages [48] along with the induction of IL-1β [49] and IL-8 [50]. NETs were also reported to enhance the polarization of anti-inflammatory macrophages as evidenced by Arg-1 expression in the presence of LPS and IFN-γ [51]. NETs reprogram IL-4/GM-CSF-induced monocyte differentiation to anti-inflammatory macrophages [52]. It is likely that NETs exert different effects on the directions of polarization of macrophages according to the environmental cues. However, the exact mechanism by which NETs act on macrophage polarization under the influence of different environmental stimuli needs further investigations. As in the case of our study, the combination of IL-4 and IL-13 with NETs provides signals driving the differentiation of CD206^{hi}MHCII^{lo} macrophages. In this scenario, the induction of MerTK led to the production of TGF-β1, the critical mediator of skin fibrosis.

In conclusion, our investigation revealed that neutrophils contribute to SSc skin fibrosis by promoting the differentiation of CD206^{hi}MHCII^{lo} macrophages through NETosis. However, we still need to understand how NETs promote the polarization of macrophages. Most importantly, the findings presented herein need to be recapitulated in patients suffering from SSc. We believe that this information is critical for understanding the pathogenesis of SSc and may lead to better designing of treatment strategies.

Declarations

Acknowledgements

This study was supported by grants from the National Key R&D Program of China (2018YFA0107500, 2021YFA1100600), National Natural Science Foundation of China (81930085, 81972682, 31961133024 and 32150710523), Jiangsu Province International Science and Technology Cooperation Program (BZ2019017), the Natural Science Foundation of Jiangsu Province (BK20211543), the State Key Laboratory of Radiation Medicine and Protection, Soochow University (GZN1201903), and National Center for International Research-Cambridge-Su Genomic Research Center (2017B01012).

Author Contributions

Pixia Gong and Yayun Ding designed this project, performed the experiments, analyzed the data, and wrote the manuscript. Wen Li, Ruifeng Tian, Yipeng Zhou and Tingting Wang conducted the in vitro experiments. Xiao Su, Junjie Jiang, Rui Liu, Jiankai Fang and Chao Feng conducted the in vivo experiments, provided advices of flow cytometry analysis and confocal microscopy analysis. Yufang Shi, Changshun Shao and Peishan Li supervised the project, designed the experiments and modified the manuscript.

Conflict of Interest

The authors declare that they have no conflict of interest.

Data availability

The data underlying this article are available in the article and in its online supplementary material.

References

1. Denton CP, Khanna D. Systemic sclerosis. The Lancet. 2017;390(10103):1685-99.
2. Henderson NC, Rieder F, Wynn TA. Fibrosis: from mechanisms to medicines. Nature. 2020;587(7835):555-66.
3. O'Reilly S. Innate immunity in systemic sclerosis. Clinical and experimental immunology. 2020;201(1):12-3.
4. Dick SA, Wong A, Hamidzada H, Nejat S, Nechanitzky R, Vohra S, et al. Three tissue resident macrophage subsets coexist across organs with conserved origins and life cycles. Sci Immunol. 2022;7(67):eabf7777.
5. Wynn TA, Vannella KM. Macrophages in Tissue Repair, Regeneration, and Fibrosis. Immunity. 2016;44(3):450-62.
6. Mantovani A, Biswas SK, Galdiero MR, Sica A, Locati M. Macrophage plasticity and polarization in tissue repair and remodelling. The Journal of pathology. 2013;229(2):176-85.

7. Wang Y, Zhang L, Wu GR, Zhou Q, Yue H, Rao LZ, et al. MBD2 serves as a viable target against pulmonary fibrosis by inhibiting macrophage M2 program. Science advances. 2021;7(1).
8. Spiller KL, Anfang RR, Spiller KJ, Ng J, Nakazawa KR, Daulton JW, et al. The role of macrophage phenotype in vascularization of tissue engineering scaffolds. Biomaterials. 2014;35(15):4477-88.
9. van der Kroef M, Carvalheiro T, Rossato M, de Wit F, Cossu M, Chouri E, et al. CXCL4 triggers monocytes and macrophages to produce PDGF-BB, culminating in fibroblast activation: Implications for systemic sclerosis. Journal of autoimmunity. 2020;111:102444.
10. Frantz C, Pezet S, Avouac J, Allanore Y. Soluble CD163 as a Potential Biomarker in Systemic Sclerosis. Disease markers. 2018;2018:8509583.
11. Ototake Y, Yamaguchi Y, Asami M, Komitsu N, Akita A, Watanabe T, et al. Downregulated IRF8 in Monocytes and Macrophages of Patients with Systemic Sclerosis May Aggravate the Fibrotic Phenotype. The Journal of investigative dermatology. 2021;141(8):1954-63.
12. Lescoat A, Lecureur V, Varga J. Contribution of monocytes and macrophages to the pathogenesis of systemic sclerosis: recent insights and therapeutic implications. Current opinion in rheumatology. 2021;33(6):463-70.
13. Higashi-Kuwata N, Jinnin M, Makino T, Fukushima S, Inoue Y, Muchemwa FC, et al. Characterization of monocyte/macrophage subsets in the skin and peripheral blood derived from patients with systemic sclerosis. Arthritis Res Ther. 2010;12(4):R128.
14. Allanore Y, Simms R, Distler O, Trojanowska M, Pope J, Denton CP, et al. Systemic sclerosis. Nature reviews Disease primers. 2015;1:15002.
15. Lescoat A, Ballerie A, Jouneau S, Fardel O, Vernhet L, Jego P, et al. M1/M2 polarisation state of M-CSF blood-derived macrophages in systemic sclerosis. Ann Rheum Dis. 2019;78(11):e127.
16. Soldano S, Trombetta AC, Contini P, Tomatis V, Ruaro B, Brizzolara R, et al. Increase in circulating cells coexpressing M1 and M2 macrophage surface markers in patients with systemic sclerosis. Ann Rheum Dis. 2018;77(12):1842-5.
17. Trombetta AC, Soldano S, Contini P, Tomatis V, Ruaro B, Paolino S, et al. A circulating cell population showing both M1 and M2 monocyte/macrophage surface markers characterizes systemic sclerosis patients with lung involvement. Respiratory research. 2018;19(1):186.
18. Yamamoto T. Animal model of systemic sclerosis. J Dermatol. 2010;37(1):26-41.
19. Pyonteck SM, Akkari L, Schuhmacher AJ, Bowman RL, Sevenich L, Quail DF, et al. CSF-1R inhibition alters macrophage polarization and blocks glioma progression. Nature medicine. 2013;19(10):1264-72.
20. Tamoutounour S, Guilliams M, Montanana Sanchis F, Liu H, Terhorst D, Malosse C, et al. Origins and functional specialization of macrophages and of conventional and monocyte-derived dendritic cells in mouse skin. Immunity. 2013;39(5):925-38.
21. Schyns J, Bai Q, Ruscitti C, Radermecker C, De Schepper S, Chakarov S, et al. Non-classical tissue monocytes and two functionally distinct populations of interstitial macrophages populate the mouse lung. Nature communications. 2019;10(1):3964.

22. Bellan M, Cittone MG, Tonello S, Rigamonti C, Castello LM, Gavelli F, et al. Gas6/TAM System: A Key Modulator of the Interplay between Inflammation and Fibrosis. International journal of molecular sciences. 2019;20(20).
23. Cai B, Dongiovanni P, Corey KE, Wang X, Shmarakov IO, Zheng Z, et al. Macrophage MerTK Promotes Liver Fibrosis in Nonalcoholic Steatohepatitis. Cell metabolism. 2020;31(2):406-21 e7.
24. Bosurgi L, Cao YG, Cabeza-Cabrerizo M, Tucci A, Hughes LD, Kong Y, et al. Macrophage function in tissue repair and remodeling requires IL-4 or IL-13 with apoptotic cells. Science. 2017;356(6342):1072-6.
25. Bouchery T, Harris N. Neutrophil-macrophage cooperation and its impact on tissue repair. Immunology and cell biology. 2019;97(3):289-98.
26. Russo RC, Garcia CC, Teixeira MM, Amaral FA. The CXCL8/IL-8 chemokine family and its receptors in inflammatory diseases. Expert review of clinical immunology. 2014;10(5):593-619.
27. Eash KJ, Greenbaum AM, Gopalan PK, Link DC. CXCR2 and CXCR4 antagonistically regulate neutrophil trafficking from murine bone marrow. The Journal of clinical investigation. 2010;120(7):2423-31.
28. Brown M, O'Reilly S. The immunopathogenesis of fibrosis in systemic sclerosis. Clinical and experimental immunology. 2019;195(3):310-21.
29. Tang PM, Nikolic-Paterson DJ, Lan HY. Macrophages: versatile players in renal inflammation and fibrosis. Nat Rev Nephrol. 2019;15(3):144-58.
30. Laskin DL, Malaviya R, Laskin JD. Role of Macrophages in Acute Lung Injury and Chronic Fibrosis Induced by Pulmonary Toxicants. Toxicological sciences : an official journal of the Society of Toxicology. 2019;168(2):287-301.
31. Lafuse WP, Wozniak DJ, Rajaram MVS. Role of Cardiac Macrophages on Cardiac Inflammation, Fibrosis and Tissue Repair. Cells. 2020;10(1).
32. Sun YY, Li XF, Meng XM, Huang C, Zhang L, Li J. Macrophage Phenotype in Liver Injury and Repair. Scandinavian journal of immunology. 2017;85(3):166-74.
33. Wen Y, Yan HR, Wang B, Liu BC. Macrophage Heterogeneity in Kidney Injury and Fibrosis. Frontiers in immunology. 2021;12:681748.
34. Kim SY, Nair MG. Macrophages in wound healing: activation and plasticity. Immunology and cell biology. 2019;97(3):258-67.
35. Gieseck RL, 3rd, Wilson MS, Wynn TA. Type 2 immunity in tissue repair and fibrosis. Nature reviews Immunology. 2018;18(1):62-76.
36. Haub J, Roehrig N, Uhrin P, Schabbauer G, Eulberg D, Melchior F, et al. Intervention of Inflammatory Monocyte Activity Limits Dermal Fibrosis. The Journal of investigative dermatology. 2019;139(10):2144-53.
37. Camenisch TD, Koller BH, Earp HS, Matsushima GK. A novel receptor tyrosine kinase, Mer, inhibits TNF-alpha production and lipopolysaccharide-induced endotoxic shock. Journal of immunology

(Baltimore, Md : 1950). 1999;162(6):3498-503.
38. Alciato F, Sainaghi PP, Sola D, Castello L, Avanzi GC. TNF-alpha, IL-6, and IL-1 expression is inhibited by GAS6 in monocytes/macrophages. Journal of leukocyte biology. 2010;87(5):869-75.
39. Rothlin CV, Ghosh S, Zuniga EI, Oldstone MB, Lemke G. TAM receptors are pleiotropic inhibitors of the innate immune response. Cell. 2007;131(6):1124-36.
40. Morse C, Tabib T, Sembrat J, Buschur KL, Bittar HT, Valenzi E, et al. Proliferating SPP1/MERTK-expressing macrophages in idiopathic pulmonary fibrosis. Eur Respir J. 2019;54(2).
41. Rovati L, Kaneko N, Pedica F, Monno A, Maehara T, Perugino C, et al. Mer tyrosine kinase as a possible link between resolution of inflammation and tissue fibrosis in IgG4-related disease. Rheumatology (Oxford). 2021;60(10):4929-41.
42. Cai B, Dongiovanni P, Corey KE, Wang X, Shmarakov IO, Zheng Z, et al. Macrophage MerTK Promotes Liver Fibrosis in Nonalcoholic Steatohepatitis. Cell metabolism. 2020;31(2):406-21.e7.
43. Kawano M, Nagata S. Efferocytosis and autoimmune disease. International immunology. 2018;30(12):551-8.
44. Gerlach BD, Ampomah PB, Yurdagul A, Jr., Liu C, Lauring MC, Wang X, et al. Efferocytosis induces macrophage proliferation to help resolve tissue injury. Cell metabolism. 2021;33(12):2445-63.e8.
45. Zawrotniak M, Rapala-Kozik M. Neutrophil extracellular traps (NETs) - formation and implications. Acta biochimica Polonica. 2013;60(3):277-84.
46. Liu L, Mao Y, Xu B, Zhang X, Fang C, Ma Y, et al. Induction of neutrophil extracellular traps during tissue injury: Involvement of STING and Toll-like receptor 9 pathways. Cell proliferation. 2019;52(3):e12579.
47. Skaug B, Assassi S. Type I interferon dysregulation in Systemic Sclerosis. Cytokine. 2020;132:154635.
48. Wei X, Zou S, Xie Z, Wang Z, Huang N, Cen Z, et al. EDIL3 deficiency ameliorates adverse cardiac remodeling by neutrophil extracellular traps (NET)-mediated macrophage polarization. Cardiovasc Res. 2021.
49. Warnatsch A, Ioannou M, Wang Q, Papayannopoulos V. Inflammation. Neutrophil extracellular traps license macrophages for cytokine production in atherosclerosis. Science. 2015;349(6245):316-20.
50. An Z, Li J, Yu J, Wang X, Gao H, Zhang W, et al. Neutrophil extracellular traps induced by IL-8 aggravate atherosclerosis via activation NF-κB signaling in macrophages. Cell cycle (Georgetown, Tex). 2019;18(21):2928-38.
51. Eghbalzadeh K, Georgi L, Louis T, Zhao H, Keser U, Weber C, et al. Compromised Anti-inflammatory Action of Neutrophil Extracellular Traps in PAD4-Deficient Mice Contributes to Aggravated Acute Inflammation After Myocardial Infarction. Frontiers in immunology. 2019;10:2313.
52. Guimarães-Costa AB, Rochael NC, Oliveira F, Echevarria-Lima J, Saraiva EM. Neutrophil Extracellular Traps Reprogram IL-4/GM-CSF-Induced Monocyte Differentiation to Anti-inflammatory Macrophages. Frontiers in immunology. 2017;8:523.

Figures

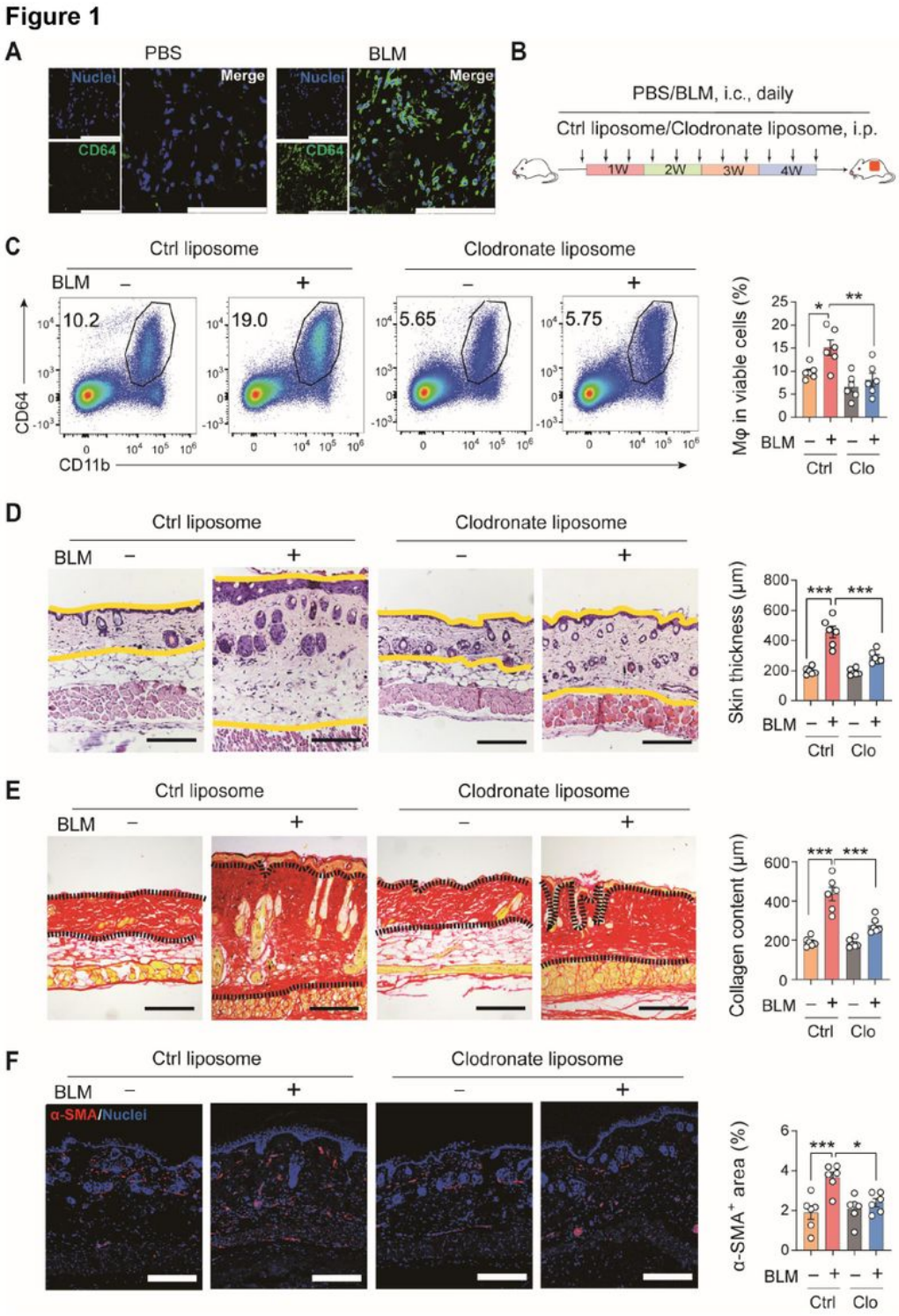

1

Figure 1

Macrophages are key contributors to skin fibrosis during SSc.

A, Mice were i.c. injected with BLM or PBS daily for 4 weeks. The infiltration of macrophages in the skin was assessed by immunofluorescence staining of CD64 on day 30. **B**, Experimental design of the BLM-induced SSc mouse model and Clodronate liposome (Clo)/Control liposome (Ctrl) treatment. Mice were sacrificed on day 30. n = 6 mice for each group. **C**, Depletion efficiency of Clo treatment on macrophages ($CD11b^+CD64^+$, pre-gate $CD45^+$ cells) in the skin was analyzed by flow cytometry on day 30. **D**, H&E staining of the skin sections (left). The distance between two yellow lines was assessed (right). Scale bars, 200 μm. **E**, Sirius red staining of the skin sections (left). The distance between two black dotted lines was assessed (right). Scale bars, 200 μm. **F**, Immunofluorescence staining of α-SMA (red) in the skin sections (left). The percentage of $α\text{-}SMA^+$ area was assessed (right). Scale bars, 200 μm. Data are representative of three experiments with similar results, and the calculated data are shown as the mean ± SEM values. $^*P < 0.05$; $^{**}P < 0.01$; $^{***}P < 0.001$; ns, not significant.

Figure 2

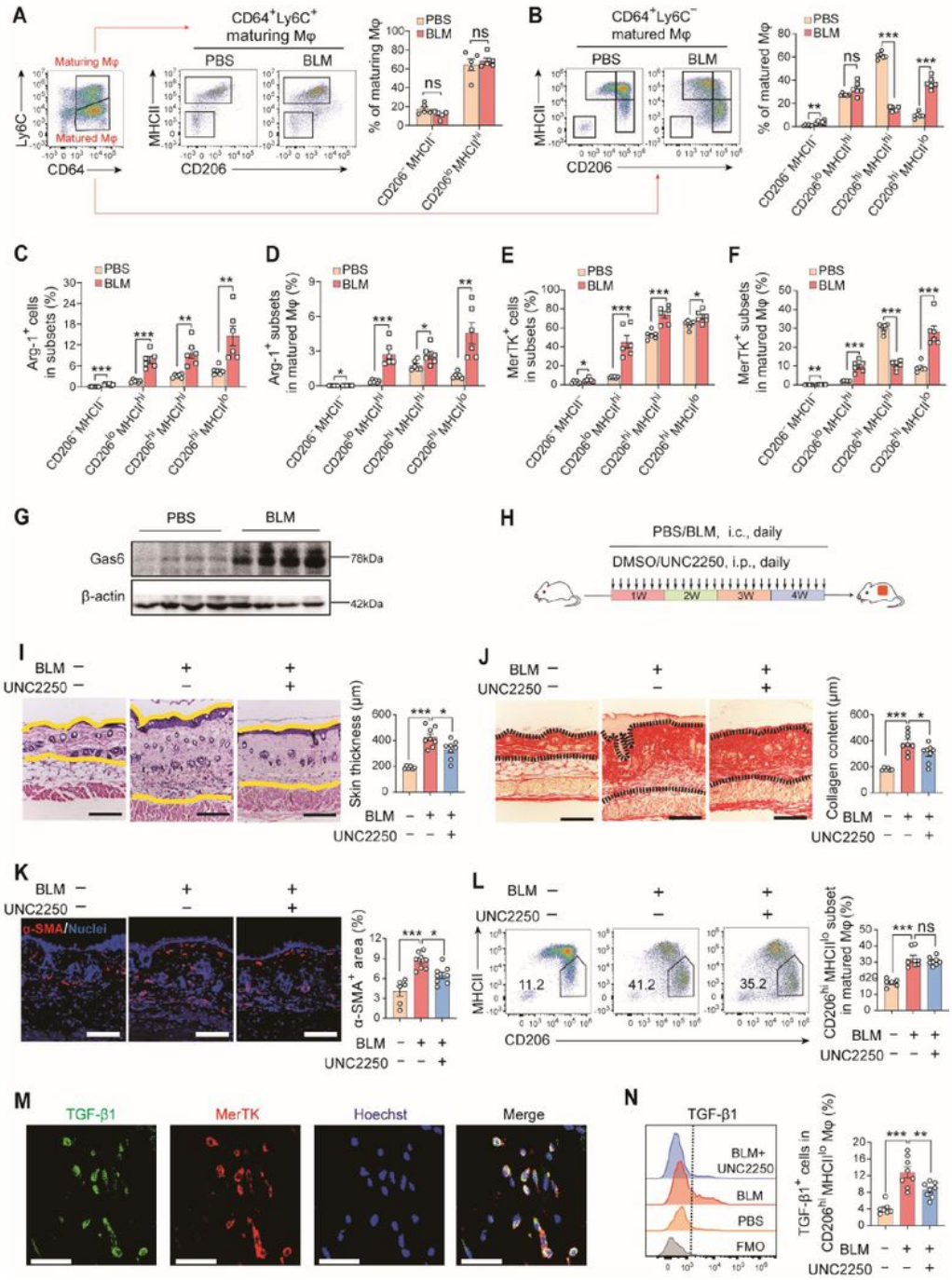

2

Figure 2

CD206^{hi}MHCII^{lo} macrophages promote SSc skin fibrosis via MerTK signaling.

A, The subsets of CD64^{+}Ly6C^{+} maturing macrophages in BLM-treated or untreated mice were classified and quantified by flow cytometry on day 30 according to the expression of CD206 and MHCII. n = 5 mice for each group. **B**, The subsets of CD64^{+}Ly6C^{-} matured macrophages in BLM-treated or untreated mice

were classified and quantified by flow cytometry on day 30 according to the expression of CD206 and MHCII. n = 6 mice for each group. **C**, Arg-1 expression in 4 subsets of $CD64^{+}Ly6C^{-}$ matured macrophages from BLM-treated or untreated mice on day 30 was analyzed by flow cytometry. n = 6 mice for each group. **D**, The percentage of $Arg\text{-}1^{+}$ subsets in $CD64^{+}Ly6C^{-}$ matured macrophages was determined. n = 6 mice for each group. **E**, MerTK expression among 4 subsets of $CD64^{+}Ly6C^{-}$ matured macrophages from BLM-treated or untreated mice on day 30 was analyzed by flow cytometry. n = 6 mice for each group. **F**, The percentage of $MerTK^{+}$ subsets in $CD64^{+}Ly6C^{-}$ matured macrophages was determined. n = 6 mice for each group. **G**, The expression of Gas6 in the whole skin lysates of BLM-treated or untreated mice on day 30 was determined by Western blotting, and each band represents a different skin sample. **H**, Experimental design of the BLM-induced SSc mouse model and MerTK inhibitor UNC2250 or DMSO treatment. Mice were sacrificed on day 30. n = 6-8 mice for each group. **I**, H&E staining of the skin sections (left). The distance between two yellow lines was assessed (right). Scale bars, 200 μm. **J**, Sirius red staining of the skin sections (left). The distance between two black dotted lines was assessed (right). Scale bars, 200 μm. **K**, Immunofluorescence staining of α-SMA (red) in the skin sections (left). The percentage of $\alpha\text{-}SMA^{+}$ area was assessed (right). Scale bars, 200 μm. **L**, Flow cytometry analysis of the effects of the MerTK inhibitor UNC2250 or DMSO on $CD206^{hi}MHCII^{lo}$ macrophages. **M**, The colocalization of MerTK (red) and TGF-β1 (green) in BLM-treated mice on day 30 was determined by immunofluorescence staining. Scale bars, 25 μm. **N**, The effect of UNC2250 or DMSO on TGF-β1 production in $CD206^{hi}MHCII^{lo}$ macrophages was analyzed by flow cytometry. Data are representative of two or three experiments with similar results, and the calculated data are shown as the mean ± SEM values. $*P < 0.05$; $**P < 0.01$; $***P < 0.001$; ns, not significant.

Figure 3

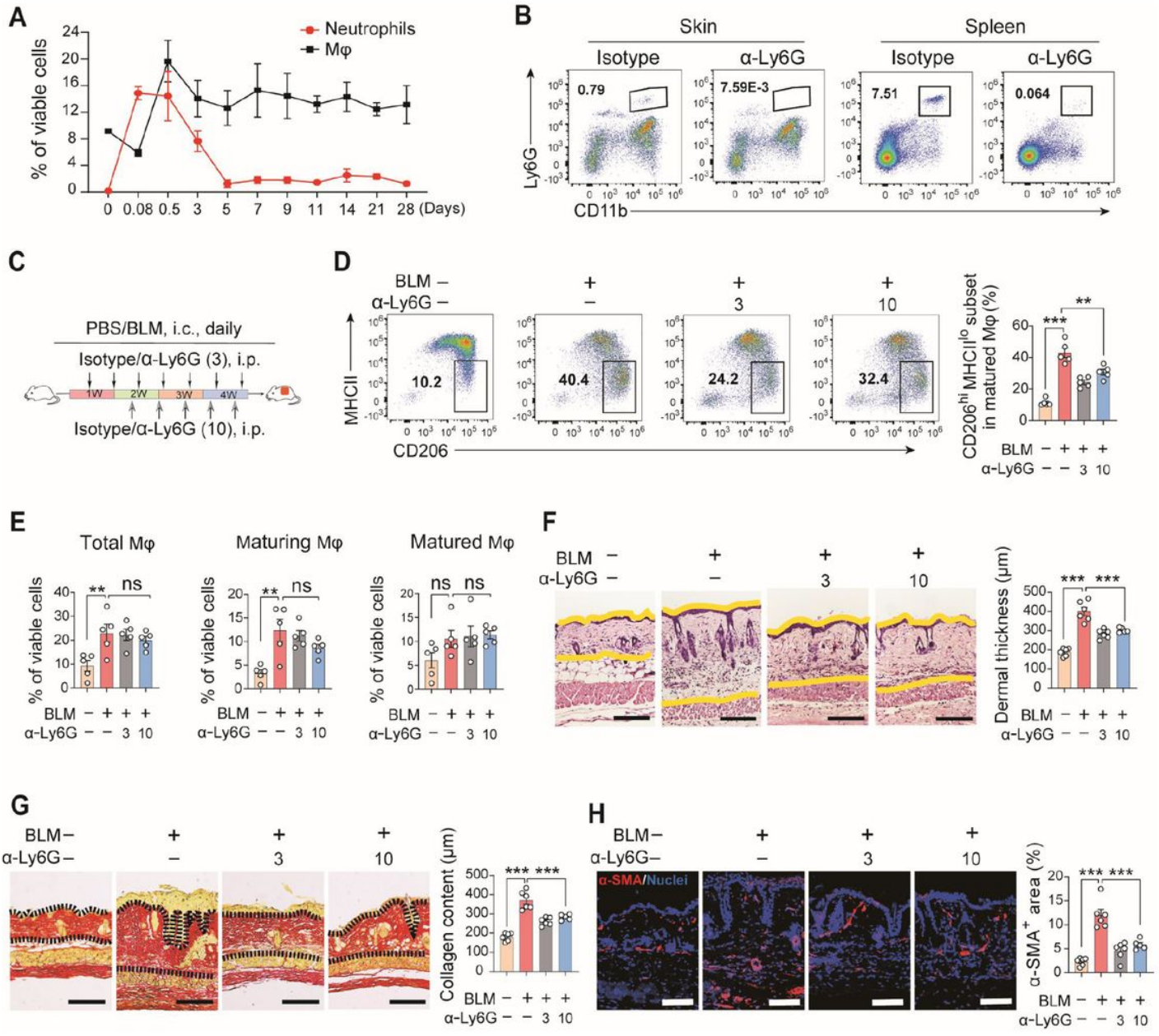

Figure 3

Neutrophil depletion inhibits the differentiation of CD206^{hi}MHCII^{lo} macrophages.

A, Mice were i.c. injected with BLM daily, and the infiltration kinetics of neutrophils (CD11b^{+}Ly6G^{+}) and macrophages (CD11b^{+}CD64^{+}) in the skin at the indicated time points were examined by flow cytometry. n = 3-5 mice for each time point. **B**, Mice were i.p. injected with anti-Ly6G antibody, and the depletion efficiency of neutrophils in the skin (left) and spleen (right) was analyzed by flow cytometry 3 days later. **C**, Experimental outline of the BLM-induced SSc mouse model and anti-Ly6G antibody or isotype

treatment. Mice were administered with anti-Ly6G antibody or isotype starting on day 3 or day 10 and repeated every 4 days throughout the whole course of SSc induction. Then mice were sacrificed on day 30. n = 5 mice for each group. **D**, The effect of neutrophil depletion on the differentiation of $CD206^{hi}MHCII^{lo}$ macrophages in BLM-treated or untreated mice was examined by flow cytometry. **E**, The effects of neutrophil depletion on the infiltration of total macrophages (left), $CD64^{+}Ly6C^{+}$ maturing macrophages (middle) or $CD64^{+}Ly6C^{-}$ matured macrophages (right) in BLM-treated or untreated mice were examined by flow cytometry. **F**, H&E staining of the skin sections (left). The distance between two yellow lines was assessed (right). Scale bars, 200 μm. **G**, Sirius red staining of the skin sections (left). The distance between two black dotted lines was assessed (right). Scale bars, 200 μm. **H**, Immunofluorescence staining of α-SMA (red) in the skin sections (left). The percentage of $α\text{-}SMA^{+}$ area was assessed (right). Scale bars, 200 μm. Data are representative of two or three experiments with similar results, and the calculated data are shown as the mean ± SEM values. $^{*}P < 0.05$; $^{**}P < 0.01$; $^{***}P < 0.001$; ns, not significant.

Figure 4

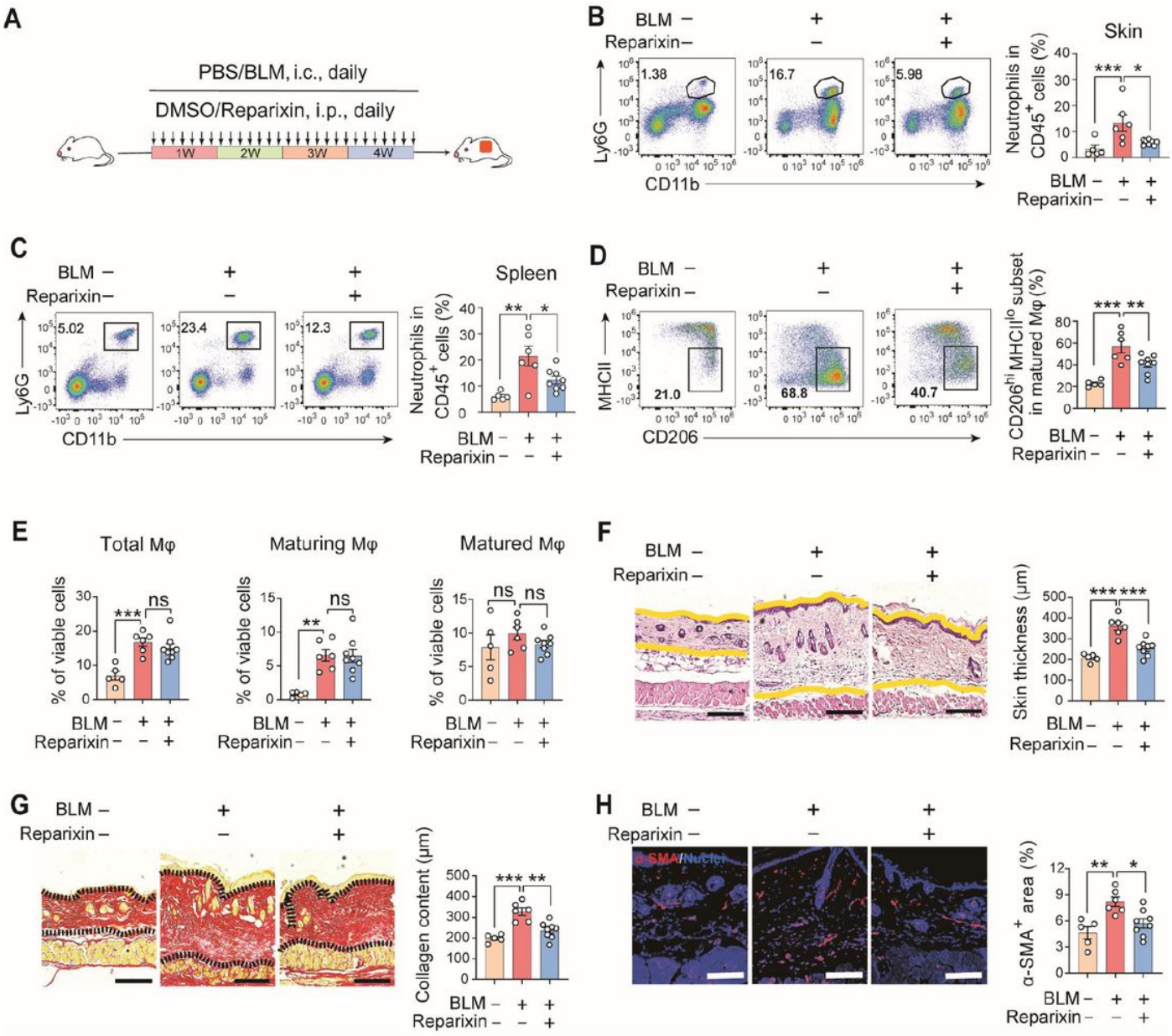

Figure 4

Inhibition of CXCR1/2 reduced CD206^{hi}MHCII^{lo} macrophages.

A, Experimental design of the BLM-induced SSc mouse model and CXCR1/2 inhibitor reparixin or DMSO treatment. Mice were sacrificed on day 30. n = 5-8 mice for each group. **B**, The percentage of neutrophils in skin was analyzed by flow cytometry. **C**, The percentage of neutrophils in the spleen was analyzed by flow cytometry. **D**, The effect of CXCR1/2 inhibition by reparixin on the differentiation of CD206^{hi}MHCII^{lo} macrophages in BLM-treated or untreated mice was analyzed by flow cytometry. **E**, The effects of reparixin on the infiltration of total macrophages (left), CD64^{+}Ly6C^{+} maturing macrophages (middle) or

$CD64^+Ly6C^-$ matured macrophages (right) in BLM-treated or untreated mice were analyzed by flow cytometry. **F**, H&E staining of the skin sections (left). The distance between two yellow lines was assessed (right); scale bars, 200 μm. **G**, Sirius red staining of the skin sections (left). The distance between two black dotted lines was assessed (right). Scale bars, 200 μm. **H**, Immunofluorescence staining of α-SMA (red) in the skin sections (left). The percentage of $\alpha\text{-SMA}^+$ area was assessed (right); scale bars, 200 μm. n = 5-8 mice for each group. Data are representative of three experiments with similar results, and the calculated data are shown as the mean ± SEM values. $^*P < 0.05$; $^{**}P < 0.01$; $^{***}P < 0.001$; ns, not significant.

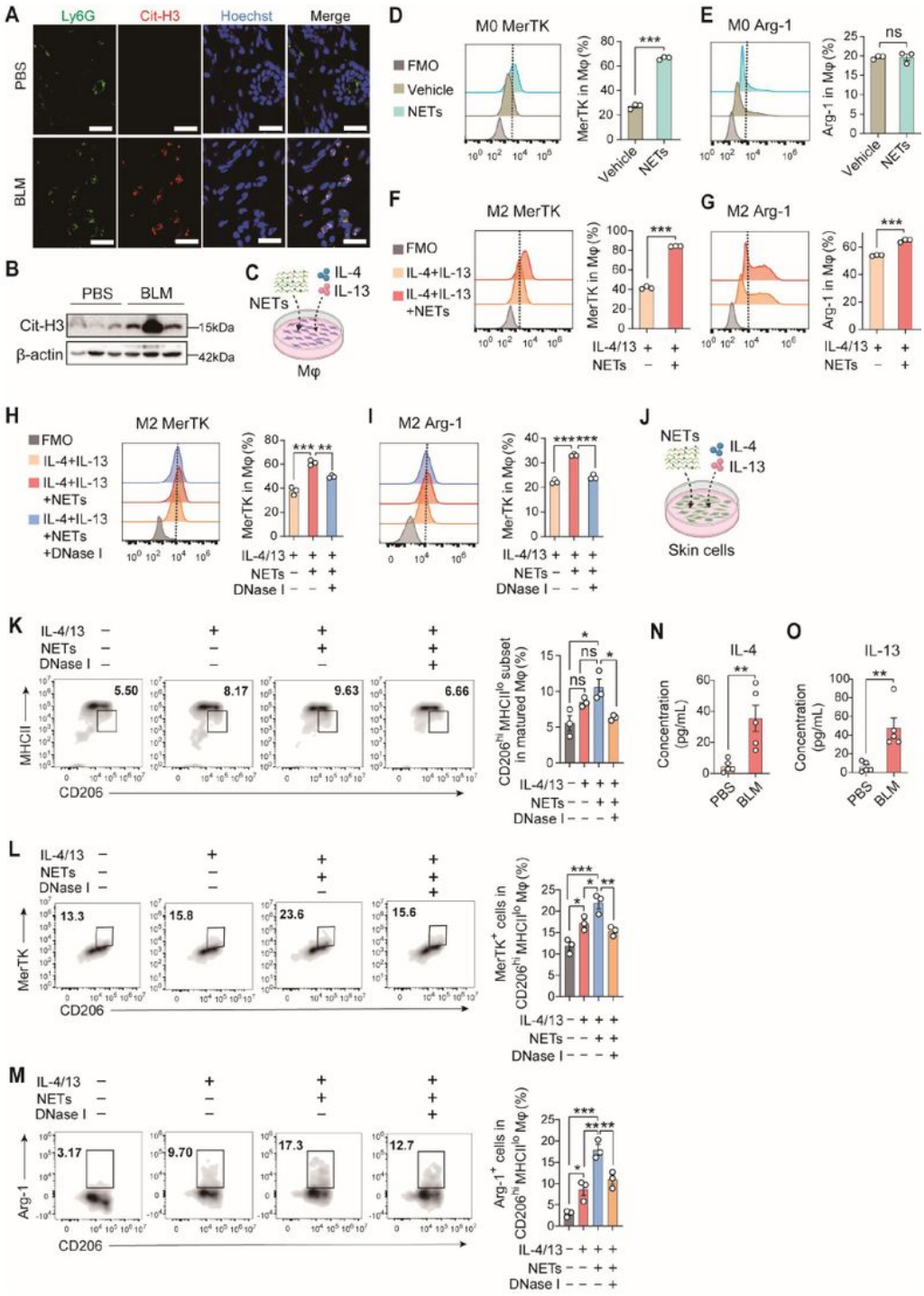

5

Figure 5

Neutrophil released NETs promote the differentiation of CD206^{hi}MHCII^{lo} macrophages.

A, Mice were i.c. injected with BLM daily for 4 weeks and sacrificed on day 30. The colocalization of Ly6G (green) and Cit-H3 (NETs marker, red) in the skin of BLM-treated or untreated mice on day 30 was detected by immunofluorescence staining. Scale bars, 50 μm. **B**, Cit-H3 expression in the whole skin

lysates of each group was detected by Western blotting analysis, and each band represents a different skin sample. **C**, A total of 1×10^6 bone marrow-derived macrophages (BMDMs) were cocultured with or without NETs generated by 2×10^6 neutrophils for 24 h in the presence or absence of IL-4 (20 ng/mL) and IL-13 (20 ng/mL). n = 3. **D**, BMDMs (M0) were cocultured with or without NETs for 24 h, and then the expression of MerTK was assayed by flow cytometry. **E**, BMDMs (M0) were cocultured with or without NETs for 24 h, and the expression of Arg-1 was assayed by flow cytometry. **F**, BMDMs were cocultured with or without NETs in the presence of IL-4 and IL-13 (M2) for 24 h, and then the expression of MerTK was assayed by flow cytometry. **G**, BMDMs were cocultured with or without NETs in the presence of IL-4 and IL-13 (M2) for 24 h, and then the expression of Arg-1 was assayed by flow cytometry. **H**, BMDMs were cocultured with or without NETs or DNase I-treated NETs for 24 h in the presence of IL-4 and IL-13 (M2), and the expression of MerTK was assayed by flow cytometry. **I**, BMDMs were cocultured with or without NETs or DNase I-treated NETs for 24 h in the presence of IL-4 and IL-13 (M2), and then the expression of Arg-1 was assayed by flow cytometry. **J**, A total of 4×10^6 skin single cells were cocultured with or without NETs generated by 2×10^6 neutrophils for 24 h in the presence of IL-4 (20 ng/mL) and IL-13 (20 ng/mL). n = 3. **K**, Skin single cells were cocultured with or without NETs or DNase I-treated NETs for 24 h in the presence of IL-4 and IL-13, and then the differentiation of $CD206^{hi}MHCII^{lo}$ macrophages was assayed by flow cytometry. **L**, Skin single cells were cocultured with or without NETs or DNase I-treated NETs for 24 h in the presence of IL-4 and IL-13. Then, the expression of MerTK in $CD206^{hi}MHCII^{lo}$ macrophages was assayed by flow cytometry. **M**, Skin single cells were cocultured with or without NETs or DNase I-treated NETs for 24 h in the presence of IL-4 and IL-13, and then the expression of Arg-1 in $CD206^{hi}MHCII^{lo}$ macrophages was assayed by flow cytometry. **O**, The concentration of IL-4 in the skin homogenate from BLM-treated or untreated mice on day 30 was detected by ELISA. n = 5 mice for each group. **P**, The concentration of IL-13 in the skin homogenate from BLM-treated or untreated mice on day 30 was detected by ELISA. n = 5 mice for each group. Data are representative of at least three independent experiments, and the calculated data are shown as the mean ± SD values. $^*P < 0.05$, $^{**}P < 0.01$, $^{***}P < 0.001$, ns, not significant.

Figure 6

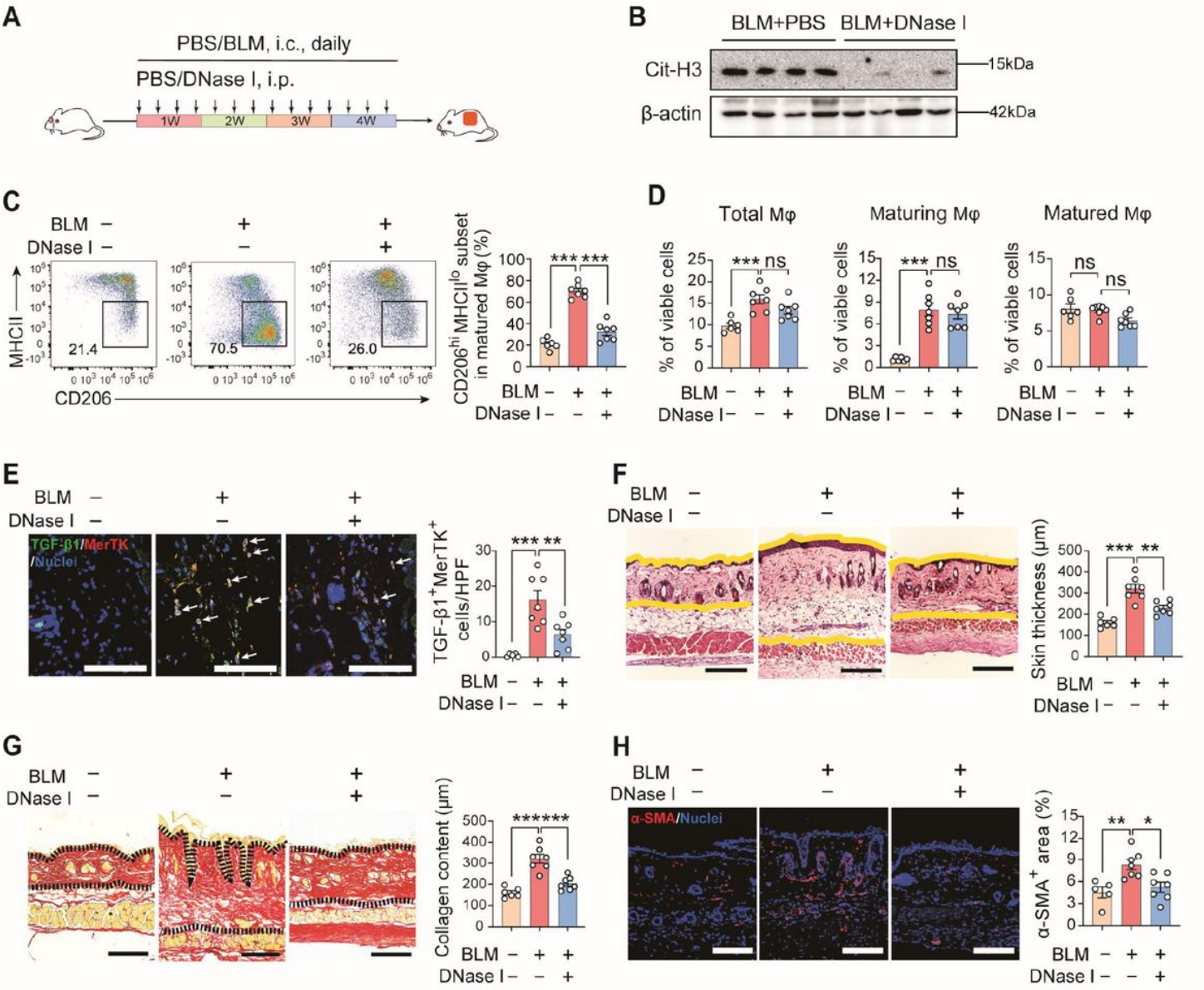

Figure 6

NETs play a critical role in skin fibrosis during SSc.

A, Experimental outline of the BLM-induced SSc mouse model and DNase I or PBS treatment. Mice were sacrificed on day 30. n = 6-7 mice for each group. **B**, Cit-H3 was examined by western blotting to evaluate the degradation efficiency of DNase I on day 30. **C**, The effect of NETs degradation by DNase I on the polarization of $CD206^{hi}MHCII^{lo}$ macrophages in BLM-treated or untreated mice was determined by flow cytometry. **E**, The effects of DNase I on the infiltration of total macrophages (left), $CD64^{+}Ly6C^{+}$ maturing macrophages (middle) or $CD64^{+}Ly6C^{-}$ matured macrophages (right) in BLM-treated or untreated mice were determined by flow cytometry. **E**, The effect of DNase I on the levels of MerTK (red) and TGF-β1

(green) in the skin was analyzed by immunofluorescence staining. Scale bars, 50 μm. **F**, H&E staining of the skin sections (left). The distance between two yellow lines was assessed (right). Scale bars, 200 μm. **G**, Sirius red staining of the skin sections (left). The distance between two black dotted lines was assessed (right). Scale bars, 200 μm. **H**, Immunostaining of α-SMA (red) in the skin sections (left). The percentage of α-SMA$^+$ area was assessed (right). Scale bars, 200 μm. Data are representative of three experiments with similar results, and the calculated data are shown as the mean ± SEM values. *P < 0.05; **P < 0.01; ***P < 0.001; ns, not significant.

Figure 7

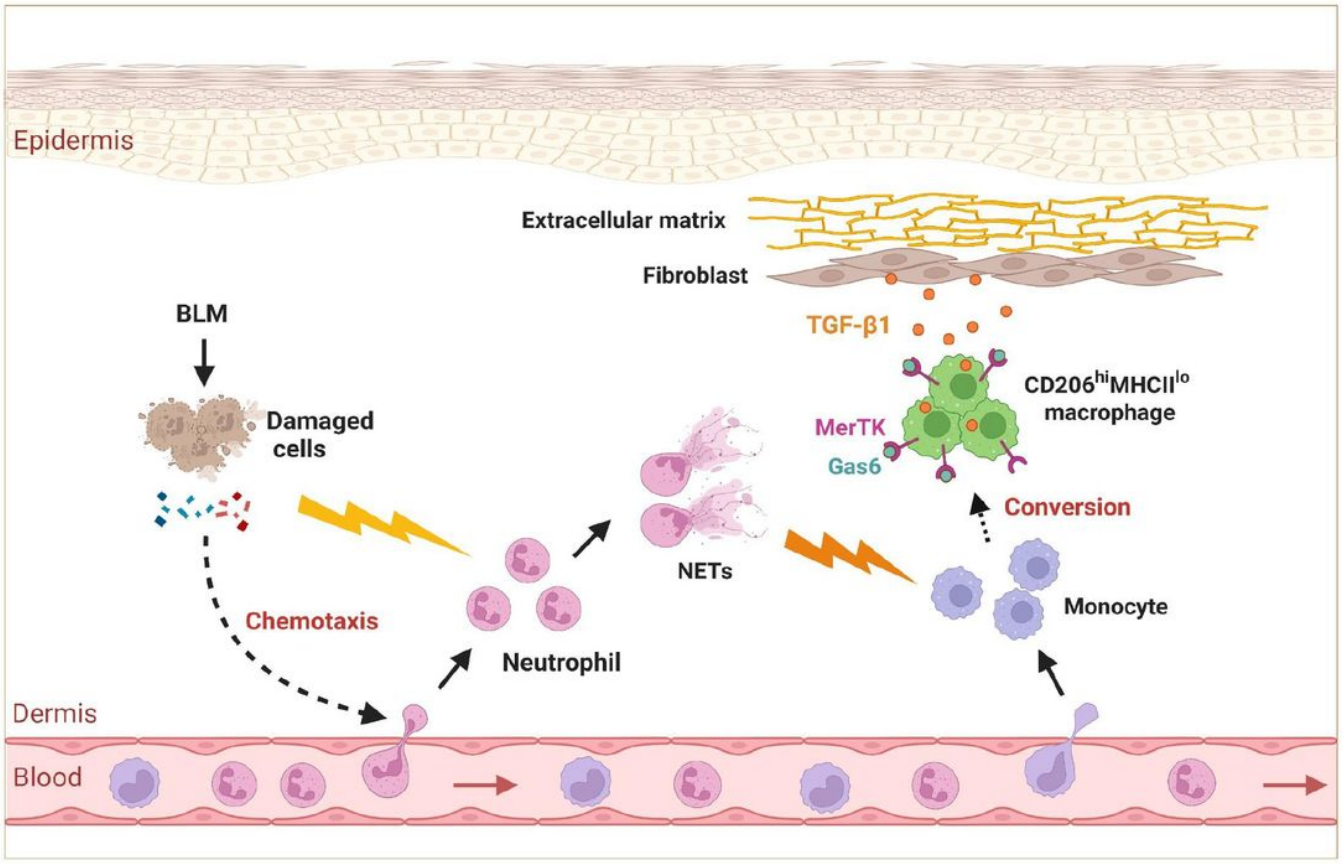

Figure 7

A diagrammatic model of the roles of neutrophils and macrophages in skin fibrosis during SSc.

Under the stimulation of BLM-damaged cells, neutrophils are substantially recruited into the dermis and release NETs, which are a prerequisite for the differentiation of profibrotic CD206^{hi}MHCII^{lo} macrophages from infiltrated monocytes. CD206^{hi}MHCII^{lo} macrophages accumulate in the dermis and mediate the profibrotic response by producing TGF-β1 in a MerTK signaling-dependent manner. The neutrophil-macrophage-fibrosis axis play a key role in the pathogenesis of SSc.

Supplementary Files

This is a list of supplementary files associated with this preprint. Click to download.

- Supplementaryinformation.pdf